

1 **Rupture process of the 2007 Niigata-ken Chuetsu-**  
2 **oki earthquake by non-linear joint inversion of**  
3 **strong motion and GPS data**  
4  
5  
6  
7  
8  
9  
10  
11  
12  
13  
14  
15  
16  
17  
18  
19

20 Cirella, A., A. Piatanesi, E. Tinti and M. Cocco  
21  
22  
23  
24

25 Istituto Nazionale di Geofisica e Vulcanologia  
26 Via di Vigna Murata 605, 00143 Roma, Italy  
27 ([cirella@ingv.it](mailto:cirella@ingv.it), [piatanesi@ingv.it](mailto:piatanesi@ingv.it), [tinti@ingv.it](mailto:tinti@ingv.it), [cocco@ingv.it](mailto:cocco@ingv.it))  
28  
29  
30  
31  
32  
33  
34  
35  
36  
37  
38  
39  
40  
41  
42  
43

44 Draft for submittal to the GRL  
45 2008  
46  
47  
48  
49

50 **Abstract**

51 We image the rupture history of the 2007 Niigata-ken Chuetsu-oki (Japan) earthquake by a  
52 nonlinear joint inversion of strong motion and GPS data, retrieving peak slip velocity,  
53 rupture time, rise time and slip direction. The inferred rupture model contains two  
54 asperities; a small patch near the nucleation and a larger one located 10–15 km to the  
55 south-west. The maximum slip ranges between 2.0 and 2.5 m and the total seismic moment  
56 is  $1.6 \times 10^{19}$  Nm. The inferred rupture history is characterized by rupture acceleration and  
57 directivity effects, which are stable features of the inverted models. These features as well  
58 as the source-to-receiver geometry are discussed to interpret the high peak ground motions  
59 observed (PGA is 1200 gals) at the Kashiwazaki-Kariwa nuclear power plant (KKNPP),  
60 situated on the hanging-wall of the causative fault. Despite the evident source effects,  
61 predicted PGV underestimates the observed values at KKNPP by nearly a factor of 10.

62

631. **Introduction**

64 The 2007 Niigata-ken Chuetsu-oki earthquake ( $M_w$  6.6) occurred near the west coast of  
65 Honshu, Japan, on July 16th at 01:13 UTC (Figure 1). The epicenter has been located at  
66  $37.557^\circ\text{N}$ ,  $138.608^\circ\text{E}$  (Japan Meteorological Agency). This earthquake caused severe  
67 damages and fatalities around the source region. In particular, the earthquake struck the  
68 Kashiwazaki-Kariwa nuclear power plant (KKNPP), placed on the hanging wall of the  
69 causative fault, where a peak ground acceleration (PGA) associated with surface motions  
70 exceeding 1200 gals has been recorded (Irikura *et al.*, 2007). The 2007 Niigata-ken  
71 Chuetsu-oki earthquake is one of the few large events whose causative fault extends  
72 beneath a nuclear power plant; for this reason it attracts the attention of both the  
73 geophysical and engineering communities. Moreover, this region was previously struck by  
74 another severe earthquake, the 2004 Mid Niigata Prefecture earthquake ( $M_w = 6.6$ ),  
75 occurred 50 km to the southeast of the hypocenter of the 2007 earthquake. Because of the

76 impact of these earthquakes and the associated hazard, the understanding of their source  
77 and rupture history is extremely important.

78 The Niigata-Kobe Tectonic Zone (NKTZ) is characterized by a compressional regime  
79 due to the convergence of the Amur plate and the Okhotsk plate. This high strain-rate zone  
80 is characterized by shortening tectonics with E-W- to NW-SE trending compressive axis  
81 (Nakajima and Hasegawa, 2007). Consistently, the focal mechanism of the 2007 Niigata-  
82 ken Chuetsu-oki earthquake, estimated by the moment tensor analysis (F-net:  
83 <http://www.fnet.bosai.go.jp>), shows reverse faulting with conjugate nodal planes dipping  
84 to NW and SE (plane 1: N215°E, 49°, 80°; plane 2: N49°E, 42°, 101° for strike dip and  
85 rake angle, respectively). The identification of rupture plane of the 2007 Niigata-ken  
86 Chuetsu-oki earthquake has been debated in the literature. Aoi *et al.* (2007) adopted both  
87 nodal planes as candidate faults for their waveform inversion approach. These authors  
88 point out that a similar fit to the recorded data can be achieved using the two nodal planes  
89 as the rupture planes. However, the spatial distribution of relocated aftershocks (e.g.,  
90 DPRI, 2007: <http://www.eqh.dpri.kyoto-ac.jp/~mori/niigata/reloc.html>) displays a fairly  
91 clear eastward dipping plane. Furthermore, recent studies (Toda, 2007; Koketsu *et al.*,  
92 2007) of the 2007 Niigata-ken Chuetsu-oki earthquake, propose the SE dipping nodal  
93 plane as the preferred fault plane. Finally, Irikura *et al.* (2007) identify the same fault plane  
94 by analyzing the aftershocks relocated using data from ocean bottom seismometers.

95 The dense strong motion seismic networks KiK-net (<http://www.kik.bosai.go.jp>) and K-  
96 NET (<http://www.k-net.bosai.go.jp>) allowed us to collect a large number of ground motion  
97 records. Data from several continuous GPS stations deployed by the Geographical Survey  
98 Institute (GSI) are also available. In this study, we investigate the rupture process of the  
99 2007 Niigata-ken Chuetsu-oki earthquake, by jointly inverting strong-motion seismic data  
100 and GPS measurements. The goal is to constrain the rupture history to better understand

101 the mechanics of the causative fault as well as the observed ground shaking at the nuclear  
102 power plant.

103

#### 1042. **Inversion methodology**

105 In order to retrieve the rupture history of the 2007 Niigata-ken Chuetsu-oki earthquake, we  
106 use a two-stage nonlinear inversion method (Piatanesi *et al.* 2007); this technique is able to  
107 jointly invert strong ground motions records and geodetic data. The extended fault is  
108 divided into subfaults with model parameters assigned at the corners; the value of every  
109 parameter is not constant inside the subfault but it spatially varies through a bilinear  
110 interpolation of the nodal values. At each point on the fault the rupture model is described  
111 by four model parameters: rise time, rupture time, peak slip velocity and rake angle. Each  
112 point on the fault can slip only once (single window approach) and the source time  
113 function can be selected among different analytical forms (e.g. box-car, triangular,  
114 exponential, regularized Yoffe) implemented in the adopted procedure (Cirella *et al.*,  
115 2007). In this study, we assume a regularized Yoffe function (Tinti *et al.*, 2005) with  $T_{acc}$   
116 (time of peak slip velocity) equal to 0.3 sec, this choice being compatible with dynamic  
117 earthquake modeling (e.g., Mikumo et al., 2003). The final slip distribution is derived by  
118 the inverted parameters and depends on the choice of the source time function and  $T_{acc}$ .

119 The nonlinear global inversion consists of two stages. In the first stage an heat-bath  
120 simulated annealing algorithm builds up the model ensemble. The algorithm starts its  
121 search by a random model and then it perturbs the model parameters one by one. Then, for  
122 each possible configuration, the forward modeling is performed with a Discrete Wave-  
123 Number technique (Spudich and Xu, 2003), whose Green's function includes the complete  
124 response of the 1-D Earth structure. Observed and predicted data are compared in the  
125 frequency domain. For strong motion data we use an objective cost function that is an  
126 hybrid representation between L1 and L2 norms, while the cost function related to the GPS

127 measurements is a sum-squared of the residuals between synthetic and recorded static  
128 displacements normalized to the observed data (equations (2) and (3) in Piatanesi *et al.*,  
129 2007). The total cost function is computed from the summation of the weighted cost  
130 functions of the two datasets. After testing the best weights' combinations with trial and  
131 error runs, in this application we have decided to adopt the same weights for the two  
132 different datasets.

133 In order to make the model ensemble independent of a particular choice of the initial  
134 model, the algorithm is conceived to perform multiple restarts with different random  
135 models. During the first stage, all models and their cost function values are saved to build  
136 up the model ensemble. In the second stage the algorithm performs a statistical analysis of  
137 the ensemble providing us the best-fitting model, the average model and the associated  
138 standard deviation (see eq.(5) and eq.(6) in Piatanesi *et al.*, 2007) computed by weighting  
139 all models of the ensemble by the inverse of their cost function values. These estimates  
140 represent the ensemble properties and are the actual solution of our nonlinear inverse  
141 problem. This approach allows us to extract the most stable features of the rupture process  
142 that are consistent with the data as well as to assess model uncertainties.

143

## 1443. **Rupture Process of the 2007 Niigata-ken Chuetsu-oki Earthquake**

145

### 146 **3.1 Data and fault model**

147 Strong motion data from 13 stations of KiK-net and K-NET and 14 GPS records of the  
148 co-seismic surface displacement (GSI) are used in our modeling attempts. Their focal  
149 distances are less than 70 km and their locations are displayed in Figure 1. We have also  
150 plotted in this figure the location of two GPS benchmarks (960566, 960567) and one  
151 accelerograph (NIG018) that are not used in the inversion presented in this study. These  
152 GPS data have been excluded because the instrumentation and/or the corrected coseismic  
153 displacements might have problems (S. Aoi and K. Koketsu, personal communications).

154 Moreover, we have not used the waveforms recorded at the NIG018 site, which is the  
155 closest to the KKNPP power plant, because it is strongly affected by non-linear site effects.  
156 However, we have verified that including or excluding these data does not change the  
157 inverted source model.

158 Original acceleration recordings are integrated to obtain ground velocity time histories.  
159 The resulting velocity waveforms are band-pass filtered between 0.02 and 0.5 Hz using a  
160 two-pole and two-pass Butterworth filter. We invert 60 seconds of each waveform,  
161 including body and surface waves. Despite the high number of triggered stations, the  
162 azimuthal coverage is limited to  $\sim 180^\circ$  due to the off-shore location of the epicenter  
163 (Figure 1). However, the results of a synthetic test (see auxiliary material) reveal that the  
164 station distribution is good enough to image model parameters.

165 The hypocenter location by H-net data is  $37.54^\circ\text{N}$ ,  $138.61^\circ\text{E}$  with 8.9 km depth  
166 (Yukutake *et al.*, 2007). We perform the inversion assuming a rupture starting point at the  
167 hypocenter located at 8 km depth and on the south-east dipping fault (Figure 1), striking  
168  $\text{N}49^\circ\text{E}$  and dipping  $42^\circ$  (F-net solution). According to aftershocks distribution we assume  
169 a fault model with a length of 38.5 km and a width of 31.5 km; the top of the fault is  
170 located at 0.5 km depth. All kinematic parameters are simultaneously inverted at nodal  
171 points every 3.5 km equally spaced along strike and dip. During the inversion, the peak  
172 slip velocity is allowed to vary between 0 and 4 m/s with 0.25 m/s step increment and the  
173 rise time between 1 and 4 sec with 0.25 step increment. The rake angle ranges between  $71^\circ$   
174 and  $131^\circ$  with  $5^\circ$  step increment (the rake angle of the moment tensor solution of F-net is  
175  $101^\circ$ ); the rupture time distribution is constrained by a rupture velocity ranging between 2  
176 and 4 km/s. To calculate the Green's functions, we adopt a 1D- crustal model referring to  
177 the velocity structure proposed by Kato *et al.* (2005).

178

## 179.2 Inversion results

180 The adopted algorithm explores about 2 millions rupture models to build up the model  
181 ensemble. Figure 2-a shows the inverted source model obtained by averaging a subset of  
182 the model ensemble (nearly 300.000 rupture models), corresponding to those models  
183 having a cost function exceeding by 2.5% the minimum value of the cost function reached  
184 during the inversion. Left panel in Figure 2-a displays the final slip distribution, middle  
185 and right panels show the rise time and the peak slip velocity distributions on the fault  
186 plane, respectively. The left panel also shows the slip direction at each grid node. The  
187 retrieved model is characterized by two principal patches of slip: a small patch near the  
188 nucleation point and a larger one located at 10÷15 km south-west from the nucleation. The  
189 larger asperity is characterized by a rise time ranging between 2.5 and 3.5 sec and a peak  
190 slip velocity of 2.0÷3.5 m/s, corresponding to 1.5÷2.5 m of slip. The inferred slip  
191 distribution and the resulting seismic moment ( $M_0 = 1.6 \times 10^{19}$  Nm) fairly agree with those  
192 inferred by Aoi *et al.* (2007).

193 The slip direction, shown in the left panel of Figure 2-a (black arrows), is consistent with a  
194 nearly pure reverse faulting mechanism. The total rupture duration is about 10 sec. In  
195 correspondence of the larger asperity, the rupture front rapidly accelerates from 2.3 km/s to  
196 3.5 km/s. The rupture acceleration occurs in the south-western portion of the fault plane,  
197 very close to KKNPP.

198 The adopted inversion methodology has the advantage to provide both the best fitting and  
199 the average source models with the corresponding standard deviations of model  
200 parameters. Figure 2-b shows the standard deviations of rupture time, rise time and peak  
201 slip velocity. We point out that the imaged acceleration of the rupture front is a stable  
202 feature and it is associated with relatively small standard deviations. As expected, standard  
203 deviations of rise time are larger in the areas of small or negligible slip. Moreover, the  
204 absolute values of peak slip velocity display a larger variability in the high slip patches.  
205 The retrieved best fitting model displays main features similar to the average one.

206 We show in Figure 2-c-d the fit to the observed data. The simulated time histories match  
207 fairly well the recorded data at most of the stations (Figure 2-c). Discrepancies at some  
208 sites can be due to the complex wave propagation in a heterogeneous medium as well as to  
209 the surface waves generated in shallow sedimentary layers not simulated in our modeling.  
210 By checking the shallow velocity structure below the recording sites, we have verified that  
211 the poor match between horizontal components of recorded and predicted waveforms at  
212 NIG013 is likely due to site amplification effects. Moreover, the fit between synthetic and  
213 observed coseismic horizontal displacement vectors at the selected GPS stations shows a  
214 good agreement (Figure 2-d). Indeed, the coseismic deformation pattern is consistent with  
215 dip slip motion, as resulting by the inferred distribution of slip direction. We have also  
216 computed and plotted in this figure the predicted displacement at the 960567 site  
217 (indicated by the dashed line), because it is close to KKNPP.

218

#### 2194. **Discussion and Conclusive remarks**

220 The main goal of this study is to image the rupture history during the 2007 Niigata-ken  
221 Chuetsu-oki earthquake by inverting available geodetic and strong motion data. However,  
222 the most peculiar feature of this earthquake is the presence of a nuclear power plant in the  
223 hanging wall of the causative fault. The inferred source model is characterized by a non-  
224 uniform slip distribution and a heterogeneous rupture propagation. Slip velocity is  
225 concentrated in two patches relatively close to the nuclear power plant (KKNPP), with a  
226 slip velocity peak of nearly  $(3.50 \pm 0.75)$  m/s. The maximum observed PGA, among the  
227 accelerograms available to the authors, is  $813 \text{ cm/s}^2$  recorded at K-NET Kashiwazaki  
228 station (NIG018), which is the closest site to KKNPP. Although the proposed model is  
229 able to fit most of the available data, it is not able to reproduce the observed amplitudes at  
230 the NIG018 site.



231 In order to quantitatively assess the source contribution to the ground shaking observed  
232 at the nuclear power plant, we have performed a forward estimate of predicted ground  
233 motions. By using the inverted rupture model, we have simulated ground velocity time  
234 histories at a virtual dense array of seismic stations (889 sites, see Figure 3-a), 14 of which  
235 correspond to the actual recording sites mapped in Figure 1. In this way we get a good  
236 azimuthal coverage and a dense sampling of the near source area. Figure 3 shows the  
237 distributions of the simulated PGV values for the fault-parallel, fault-normal and vertical  
238 components. PGV is measured from synthetic seismograms filtered in the same frequency  
239 bandwidth adopted for waveform inversion.

240 The pattern of peak ground velocity reflects the fault geometry, the heterogeneous slip  
241 distribution and rupture SW acceleration, revealing clear directivity effects. The high  
242 values of PGV predicted southwestward of the hypocenter are mostly due to the slip  
243 distribution and source-to-receiver geometry. Despite this relevant rupture directivity  
244 effect, the predicted PGV at NIG018 underestimates the observed value (filtered in the  
245 same frequency bandwidth as synthetics) by nearly a factor 10. This result confirms that  
246 other effects associated with complex propagation paths and site amplifications contributed  
247 to explain the severe ground motion recorded at KKNPP. Worthy of note is the  
248 observation that recorded PGA at KKNPP is much larger (nearly two times) than the  
249 adopted design value (Sugiyama, 2007).

250 We emphasize that the average rupture model proposed in this study by inverting GPS  
251 and strong motion data includes the most relevant features of roughly 300.000 models,  
252 which yield a reasonable fit to the observed data. In particular, the adopted inversion  
253 procedure allows us to analyze the standard deviations of model parameters and to  
254 conclude that the rupture acceleration as well as the directivity effects are stable features of  
255 the causative earthquake rupture. We believe that this approach is of relevance to constrain

256 the variability of kinematic model parameters, and it represents an important step towards  
257 the performing of reliable predictions of ground motion time histories.

258

259 **Acknowledgments.** The authors are grateful to Shin Aoi and Kazuki Koketsu for the  
260 information. Thanks to K-NET and KiK-net for providing strong motion data, and to  
261 GSI for providing GPS data. Some figures are made using Generic Mapping Tools  
262 free software (*Wessel and Smith, 1998*). We thank two anonymous referees and the  
263 editor for their useful comments.

264 **References**

265

266 Aoi, S., H. Sekiguchi, N. Morikawa, T. Ozawa, T. Kunugi, M. Shirasaka (2007),

267 Source Process of the 2007 Niigata-ken Chuetsu-oki Earthquake derived from

268 Near-fault Strong Motion Data, *Eos Trans. AGU*, 88(52), Fall Meet. Suppl.,

269 Abstract S54A-04.

270

271 Cirella, A., A. Piatanesi, P. Spudich, M. Cocco and E. Tinti (2007), Using a Global

272 Search Inversion to Constrain Earthquake Kinematic Rupture History and to

273 Assess Model Uncertainty, *Eos Trans. AGU*, 88(52), Fall Meet. Suppl., Abstract

274 S53C-03.

275

276 Irikura, K., T. Kagawa, K. Miyakoshi, S. Kurahashi (2007), Rupture process and

277 strong ground motions of the 2007 Niigataken Chuetsu-Oki earthquake –

278 Directivity pulses striking the Kashiwazaki-Kariwa Nuclear Power Plant-, *Eos*

279 *Trans. AGU*, 88(52), Fall Meet. Suppl., Abstract S31B-0441.

280

281 Kato, A., E. Kurashimo, N. Hirata, S. Sakai, T. Iwasaki and T. Kanazawa (2005),

282 Imaging the source region of the 2004 mid-Niigata prefecture earthquake and the

283 evolution of a seismogenic thrust-related fold, *Geophys. Res. Lett.*, 32, L07307,

284 doi:10.1029/2005GL022366.

285

286 Koketsu, K., H. Miyake, K. Hikima (2007), Source Inversion for the 2007 Chuetsu-

287 oki, Japan, Earthquake: A Case of Difficulty Determining the Source Fault Plane,

288 *Eos Trans. AGU*, 88(52), Fall Meet. Suppl., Abstract S54A-05.

289

290

291 Mikumo, T., K. B. Olsen, E. Fukuyama, and Y. Yagi (2002). Stress-breakdown time  
292 and slip-weakening distance inferred from slip-velocity functions on earthquake  
293 faults, *Bull. Seism. Soc. Am.*, 93(1), 264–282.  
294

295 Nakajima, J. and A. Hasegawa (2007), Deep crustal structure along the Niigata-Kobe  
296 Tectonic Zone, Japan: Its origin and segmentation, *Earth Planets Space*, 59, e5-e8.  
297

298 Piatanesi, A., A. Cirella, P. Spudich, and M. Cocco (2007), A global search inversion  
299 for earthquake kinematic rupture history: Application to the 2000 western Tottori,  
300 Japan earthquake, *J. Geophys. Res.*, 112, B07314.  
301

302 Spudich, P. and L. Xu (2003), Software for calculating earthquake ground motions  
303 from finite faults in vertically varying media, in *International Handbook of*  
304 *Earthquake and Engineering Seismology*, Academic Press.  
305

306 Sugiyama, Y (2007), 16 July 2007 Niigata-ken Chuetsu-oki earthquake; its  
307 characteristics, tectonic background and significance for active fault evaluation,  
308 *Eos Trans. AGU*, 88(52), Fall Meet. Suppl., Abstract T31G-01.  
309

310 Tinti, E., E. Fukuyama, A. Piatanesi and M. Cocco (2005), A kinematic source time  
311 function compatible with earthquake dynamics, *Bull. Seismol. Soc. Am.*, 95(4),  
312 1211-1223, doi:10.1785/0120040177.  
313

314 Toda, S. (2007), 2007 Mw=6.6 Niigata Chuetsu-Oki earthquake ruptured on a fault  
315 strongly unclamped by the 2004 Mw=6.6 Niigata Chuetsu shock, *Eos Trans. AGU*,  
316 88(52), Fall Meet. Suppl., Abstract S13B-1301.

317

318 Wessel, P. and W.H.F. Smith (1998), New, improved version of the Generic  
319 Mapping Tools released, *EOS Trans. AGU*, 79, 579.

320

321 Yukutake, Y., T. Takeda, and K.Obara (2007), Spatial distribution of aftershocks in  
322 the region of Niigata Tyuetsu-oki Earthquake in 2007, by waveform correlation  
323 analysis, *Seismol. Soc. Jpn. Programme. Abstr. Fall Meeting*, PI-063, (in  
324 Japanese).

325

326 **Figure captions**

327

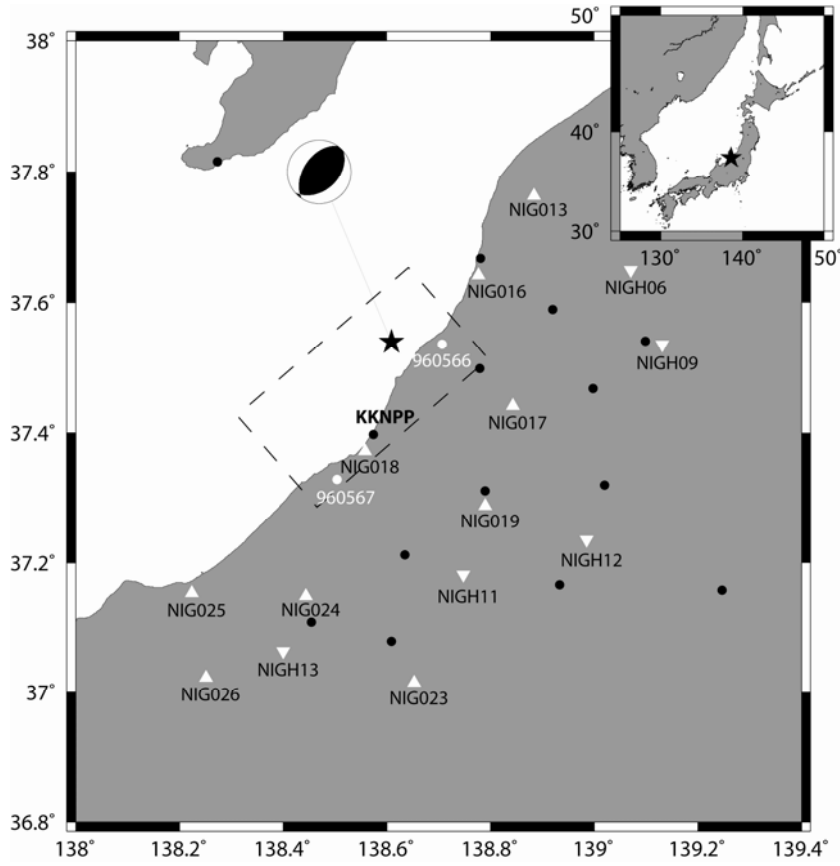
328 **Figure 1.** Map of the fault geometry of the 2007 Niigata-ken Chuetsu-oki, Japan  
329 earthquake. The dashed black line represents the surface projection of the fault plane  
330 adopted in this study. Black star indicates the epicenter. White triangles and inverted  
331 triangles represent K-NET (surface sensor) and KiK-net (borehole sensor) strong motion  
332 stations respectively. Black dots represent GPS stations. White dots are GPS stations not  
333 used in this study. KKNPP indicates the site of Kashiwazaki-Kariwa nuclear power plant.

334

335 **Figure 2.** a) Inverted rupture model (average model from ensemble inference) of the 2007  
336 Niigata-ken Chuetsu-oki earthquake. Left, middle and right panels show total slip, rise  
337 time and peak slip velocity distributions, respectively. White color in middle panel  
338 represents the areas of small or negligible slip. Rupture time shown by contour lines (in  
339 seconds); black arrows displayed in left panel represent the slip vector. b) Standard  
340 deviation of rupture time, rise time and peak slip velocity for the average rupture model  
341 computed through ensemble inference. c) Comparison of recorded strong motions (blue  
342 lines) with predicted waveforms computed from the inverted rupture model of Figure 2-a  
343 (red lines). Numbers with each trace are peak amplitude of the synthetic waveforms in  
344 cm/s. d) Comparison of observed (blue arrows) with synthetic (red arrows) horizontal GPS  
345 displacements.

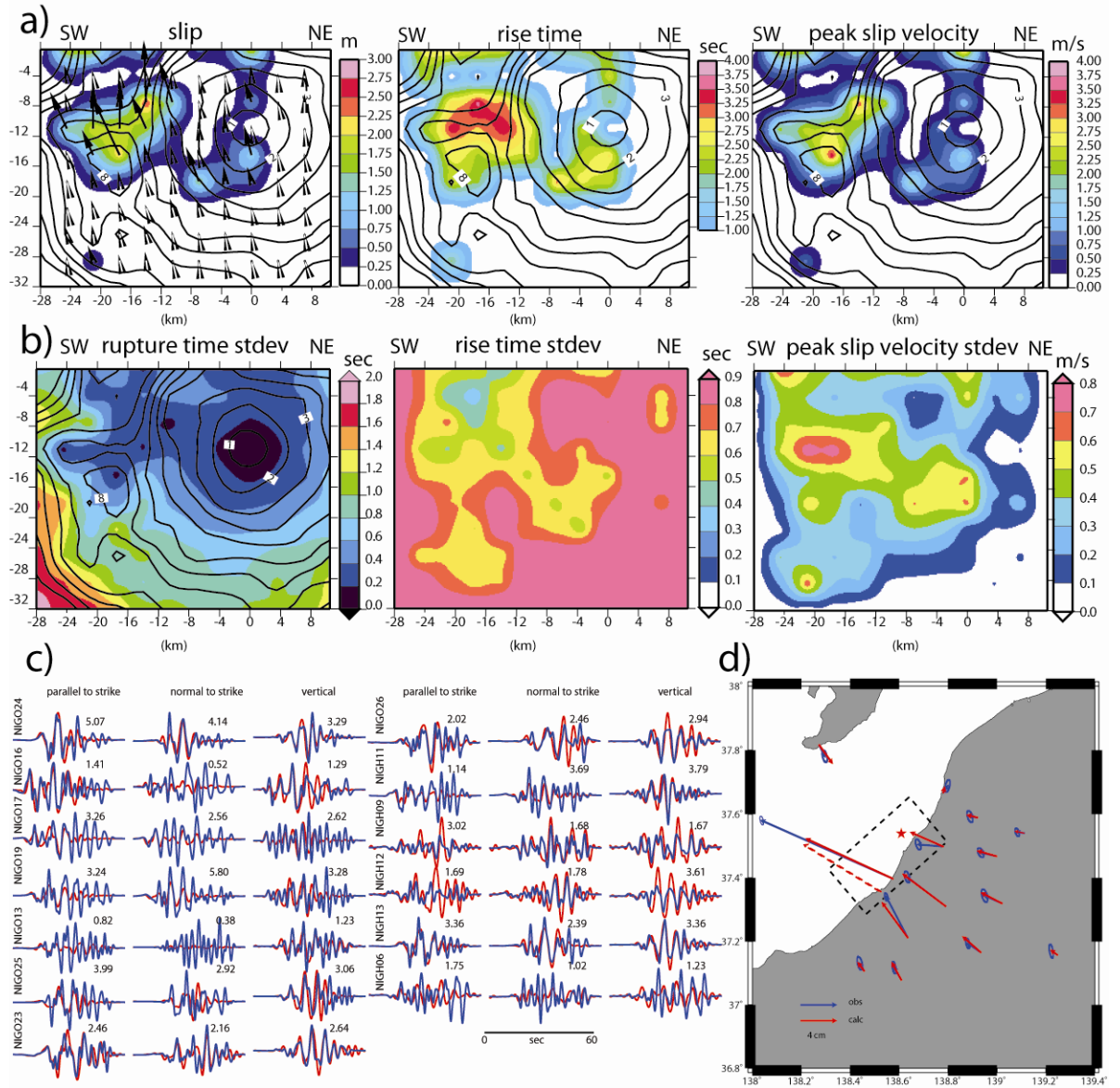
346

347 **Figure 3.** Predicted PGV distribution for the inverted model shown in Figure 2-a.  
348 Maps a), b) and c) display the parallel to strike, normal to strike and vertical  
349 component, respectively. White circles in panel a) indicate the grid of sites and the  
350 white label shows the location of the Kashiwazaki Kariwa nuclear power plant  
351 (KKNPP).



353  
354

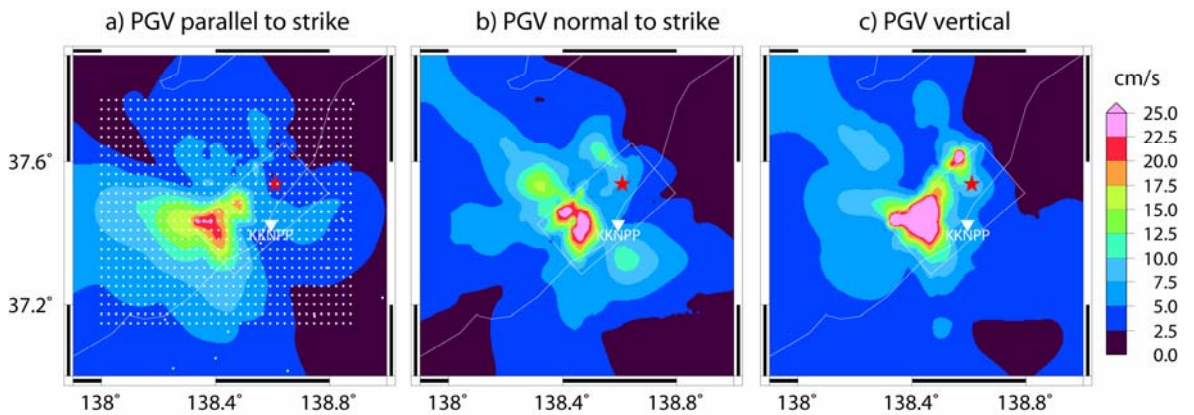
**Figure1**



355  
356

**Figure2**

357



358  
359

**Figure3**